Journal of Power Sources 211 (2012) 161–168

Contents lists available at SciVerse ScienceDirect

Journal of Power Sources

journal homepage: www.elsevier.com/locate/jpowsour

Enhancing the high-temperature proton conductivity of phosphoric acid doped poly(2,5-benzimidazole) by preblending boron phosphate nanoparticles to the raw materials

Suqing Di, Liuming Yan*, Shuaiyuan Han, Baohua Yue, Qingxia Feng, Liqing Xie, Jin Chen, Dongfang Zhang, Chao Sun

Department of Chemistry, College of Sciences, Shanghai University, 99 Shangda Road, Shanghai 200444, China

ARTICLE INFO

Article history:
Received 2 March 2012
Accepted 28 March 2012
Available online 11 April 2012

Keywords:
Proton exchange membranes
Polybenzimidazole
Boron phosphate
Proton conductivity
Methanol vapor permeability

ABSTRACT

The boron phosphate-poly(2,5-benzimidazole) (or BPO_4–ABPBI) nanocomposite proton exchange membranes were prepared by preblending BPO_4 nanoparticles to the 3,4-diaminobenzoic acid solution before its polycondensation. The phosphoric acid doped nanocomposite membrane possesses enhanced proton conductivity compared to the phosphoric acid doped pristine ABPBI membrane without BPO_4 nanoparticles; and a maximum proton conductivity of 27.3 mS cm^{-1} was observed in the phosphoric acid doped nanocomposite membrane consisting of 25% BPO_4 nanoparticles at 180 °C under anhydrous condition. The enhancement of proton conductivity is attributed to the dangling hydroxyl or geminal hydroxyl groups of the excess phosphoric acid molecules on surface of the BPO_4 nanoparticles based on density functional theory calculations. In addition, the blending of BPO_4 nanoparticles significantly decreases the methanol vapor permeability through the membrane by about two-fold.

1. Introduction

Proton exchange membrane fuel cell (PEMFC) technology is considered one of the most important energy conversion technologies for the future society when the conventional fossil fuels are substituted by renewable energies [1,2]. However, the large scale commercialization of such technology is challenged by the high cost of the electrocatalysts and the proton exchange membranes (PEMs) [3]. These seemingly economic obstacles are actually technical challenges since the best method to cut down the cost of the electrocatalysts and PEMs is to substitute cheap materials for these expensive materials. For example, by substituting a cheap high-temperature proton conducting material for the expensive poly(-perfluorosulfonic acid) (PFSA) ionomer and increasing the operational temperature of the PEMFCs to well above the boiling point of water (>120 °C), the cost for electrocatalysts can also be significantly cut down since the activities of electrocatalysts are greatly improved at elevated temperatures [3,4]. Other advantages from the high-temperature PEMFCs include improved tolerance to impurities (such as CO) in fed gas, simplified water and heat management systems, and improved overall energy conversion efficiency [5–10]. Consequently, the development of PEMs with high proton conductivities at high-temperature in water deficiency state is attracting great research interests both from the industrial corporations and academic institutions.

In order to meet the diverse requirements for high-temperature PEMFCs, the composite membrane approach has been widely employed to improve the overall performances of proton exchange membranes as the properties of the multiple components can be retained in the composite membranes. For example, by blending water retaining materials to the PFSA ionomer, the resulting composite membranes exhibits improved water retaining characteristics and proton conductivities at high-temperature [11,12]. However, these membranes cannot meet the requirement of high-temperature fuel cells operated at temperatures well above 120 °C [13]. Recently, phosphoric acid (H_3PO_4) doped poly[2,2′-(*m*-phenylene)-5,5′-bibenzimidazole] (polybenzimidazole, PBI) has attracted great research interests since its conductivity is retained even at 200 °C and under anhydrous conditions [7,14–17]. The phosphoric acid doped PBI belongs to a large group of proton conducting materials called the acid–base complexes which are generally divided into acid-doped basic polymers, base-doped acidic polymers, and acid–base polymeric complexes [18]. The pristine PBI exhibits excellent high-temperature performances owing to the strong hydrogen bonding and the π–π stacking

* Corresponding author. Tel./fax: +86 21 66132405.
E-mail address: liuming.yan@shu.edu.cn (L. Yan).

0378-7753/$ – see front matter © 2012 Elsevier B.V. All rights reserved.
doi:10.1016/j.jpowsour.2012.03.091

interaction between the aromatic heterocyclic backbones; and the protogenic component H_3PO_4 exhibits very good proton conductivity at high temperature in anhydrous state [7,19]. Other protogenic components, such as heteropoly acids [20–22], zirconium hydrogen phosphate [20], polymers bearing phosphonic acid groups or sulfonic acid groups [23,24], and other inorganic fillers [25], have also been blended to the PBI. These acid–base complexes have shown promising proton conductivity at high temperatures in water deficiency or even anhydrous state because the membrane composition can be adjusted to optimize the overall performance [20,26–28]. Poly(2,5-benzimidazole) or ABPBI has also attracted great research interests since the ABPBI is the simplest polybenzimidazole and can be synthesized by polycondensation of a single cheap monomer 3,4-diaminobenzoic acid [29–32]. The ABPBI can also be modified by sulfonation forming sulfonated ABPBI (SABPBI) [33], or by copolymerization [34], or by incorporation of phosphomolybic acid [35,36], or poly(vinylphosphonic acid) [37]. The other high-temperature PEMs based on polybenzimidazole include the poly(2,2′-(1,4-phenylene)-5,5′-bibenzimidazole) (para-PBI) [38], and copolymers [39].

Pristine boron phosphate (BPO_4), stoichiometric or non-stoichiometric, shows very low proton conductivity and high hygroscopicity [40]. As the adsorbed water molecule dissociates, the surface of BPO_4 is covered with various types of hydroxyl groups: free B–OH and P–OH, geminal P–OH and H-bonded adjacent OH groups associated with both B and P [41]. And a five-magnitude decrease in resistance was observed as the relative humidity increases from 35 to 90% [42]. The proton conductivity increases even more significantly for the non-stoichiometric BPO_4 with high P/B ratio [40]. The BPO_4 was also directly blended to sulfonated poly(ether ketone) (SPEEK) resulting a composite material with a proton conductivity of 75 mS cm^{-1} [41] and low methanol permeability [43]. If in-situ sol–gel process was applied to the preparation of the SPEEK/BPO_4 composite, a four-fold increase in proton conductivity was observed [44,45]. The sulfonated poly(-ether sulfone)/BPO_4 blend also shows promising conductivity which increases from 6.5 to 22 mS cm^{-1} at room temperature as the BPO_4 content increases from 0 to 40% [46]. A five-fold increase in proton conductivity, and excellent thermal, oxidative and hydrolytic stabilities were observed for the composite containing poly(-phthalazinone ether nitrile ketone) and 30% BPO_4 by an in-situ process [47]. The BPO_4 was also blended to SPAEK-6F and SPEEK via an in situ sol–gel process with homogeneous distribution [48]. The PEM prepared from BPO_4 and SPEEK/PBI blend exhibits a conductivity comparable to that of NAFION membrane but a much higher glass transition temperature at 220 °C [49].

Considering that BPO_4 is stable in phosphoric acid and that a high P/B ratio can facilitate the formation of surface P–OH, improved proton conductivity is expectable if the BPO_4 is blended to the phosphoric acid doped ABPBI. In this work, a high-temperature PEM based on the H_3PO_4 doped BPO_4–ABPBI nanocomposite was developed and satisfactory comprehensive performance was obtained.

2. Experimental

2.1. Materials

The 3,4-diaminobenzoic acid (DABA, 99.1%, Shanghai Yuanji Chemical Ltd.) was purified by recrystallization [50]: 10.0 g DABA was firstly dissolved in 100.0 ml deionized water, and then about 10.0 ml hydrazine hydrate ($N_2H_4 \cdot H_2O$, 85%, SCRC) was added to adjust the pH of the solution to approximately 8.10 at 70 °C. After the DABA was completely dissolved, 4.0 g active carbon (SCRC) was added to absorb impurities from the solution. Upon filtration, clear golden solution was obtained. Finally, 35% acetic acid (Aladdin Reagent Inc.) was added and DABA precipitated as light pinkish crystals (mp = 215.5 °C). Phosphorus pentoxide (P_2O_5, 98%, SCRC), methanesulfonic acid (MSA, 98%, SCRC), phosphoric acid (H_3PO_4, 85%, SCRC), and boron phosphate (BPO_4, 99%, SCRC) were used as received.

2.2. Fabrication of ABPBI and BPO_4–ABPBI nanocomposite membranes

The ABPBI solution was synthesized by polycondensation of 3.0 g DABA using 4.5 g P_2O_5 as dehydrating agent and 30.0 ml MSA as solvent at 150 °C under protection of N_2 atmosphere for 3.0 h (Scheme 1) [31]. And then, the ABPBI solution was poured on a glass plate forming a wet membrane; and the thickness of the wet membrane was controlled by a blade. Two solvent elimination processes, the direct liftoff process and the evaporation and liftoff process, were applied to the elimination of solvent from the wet membranes: In the direct liftoff process, the wet membranes were directly liftoff in deionized water and were boiled for 12 h to eliminate the phosphoric acid and residual MSA. In the evaporation and liftoff process, the wet membranes were firstly kept at 105 °C for 1 h, 150 °C for 5 h, 170 °C for 1 h in a stove for the elimination of MSA, then were liftoff in deionized water after being cooled down to room temperature, finally were boiled in water for 12 h to eliminate the phosphoric acid and residual MSA. The acid free ABPBI membranes were then immersed in 65% phosphoric acid at 70 °C for 48 h. Finally, the phosphoric acid soaked ABPBI membranes were dried at 70 °C for 3 h and were ready for the characterization of various properties.

Two preparation processes, the preblending process and post-blending process, were applied to the preparation of BPO_4–ABPBI nanocomposite membranes. In the preblending process, the BPO_4 nanoparticles were dispersed in the MSA solution of DABA under ultrasonic stirring before polycondensation. In the post-blending process, the BPO_4 nanoparticles were dispersed in the ABPBI solution by ball milling. After these steps, the BPO_4–ABPBI nanocomposite membranes were prepared using the same procedure as the pristine ABPBI membranes without BPO_4. Since nanocomposite membranes prepared from the preblending process possess higher proton conductivity than that prepared from the post-blending process, all the results reported in the following text were measured for the preblending BPO_4–ABPBI nanocomposite membranes.

2.3. Characterizations of the nanocomposite membranes

The morphological and structural characteristics of the membranes were characterized using the SEM and FTIR methods. The morphologies of the membranes were characterized using the JEOL-JMS-6700F high resolution scanning electron microscope (HRSEM). The FTIR spectra were recorded from 400 to 4000 cm^{-1} on an Avatar 370 FTIR spectrometer (Nicolet, USA). The electrical impedance spectroscopy (two-probe method with the SFF-50-3-2 shielding cable) was applied to characterize the proton conductivities of membranes in temperature range of 100–180 °C using the SI-1287 electrochemical interface and 1255B frequency response analyzer (AMETEK Inc., UK).

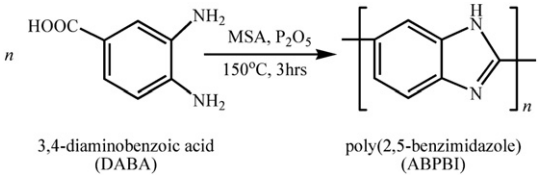

Scheme 1. Polycondensation of DABA.

The mechanical properties of the membranes were evaluated by means of ultimate tensile strengths and Young's moduli at room temperature in air. The sample membranes (about 60 μm in thickness) were firstly pretreated exactly the same way as the characterization of proton conductivity; and then, were cut into pieces about 10.0 mm in length and 4.0 mm in width in the center. The membranes were elongated at a constant speed of 1 mm per minute, and the tensile stresses were recorded as function of membrane elongation.

The permeability of methanol vapor was measured slightly above the boiling point of methanol by an apparatus consisting of two chambers as shown in Scheme 2. The major parts of the apparatus are two Γ-shaped glass tubes each attached to a three-necked flask, and the proton exchange membrane was pressed between the Γ-shaped tubes. The left flask, filled with liquid methanol, was kept at 66.0 °C slightly above the boiling point of methanol. The right flask, filled with deionized water to dissolve the methanol vapor that permeates from the membrane, was kept at room temperature. Before the starting of the measurement, the air in the left chamber was evacuated and was replaced by methanol vapor evaporated from the liquid methanol. During the process of measurement, both Γ-shaped tubes were kept at 65.5 °C in a heating jacket. The partial pressure of methanol vapor in the left Γ-shaped tube was controlled at 1.0 atm, and that in the right Γ-shaped tube was connected to atmosphere via the condenser. Finally, the permeability of methanol vapor was evaluated by determination of the moles of methanol in right flask sampled every few hours during the measurement process.

The moles of methanol crossover the membrane were determined by colorimetry using a UV-2501PC spectrophotometer. The coloration process of methanol was as follows: Firstly, the methanol was oxidized to formaldehyde by $KMnO_4$ in phosphoric acid; and then, the excess $KMnO_4$ was eliminated by addition of Na_2SO_3; finally, coloration was developed by addition of chromotropic acid and concentrated sulfuric acid [51]. For the details of the coloration process, the readers are referred to the Supplementary material.

3. Results and discussions

3.1. Morphology

The cross-sectional morphologies of the dehydrated pristine ABPBI and BPO_4–ABPBI nanocomposite membranes, and phosphoric acid doped pristine ABPBI and BPO_4–ABPBI nanocomposite membranes were shown in Fig. 1. For the dehydrated pristine ABPBI membranes prepared using the direct liftoff process, irregular structures are observed with characteristic dimension of about 100 nm (Fig. 1a); while for that prepared using the evaporation and liftoff process, the structures with characteristic dimension of about 30 nm are observed (Fig. 1b). Thus, the elimination of MSA from wet membranes before liftoff in deionized water can result denser membrane than that without elimination of MSA. On the other hand, the porosity of the membrane prepared using the direct liftoff process is higher than that prepared using the evaporation and liftoff process.

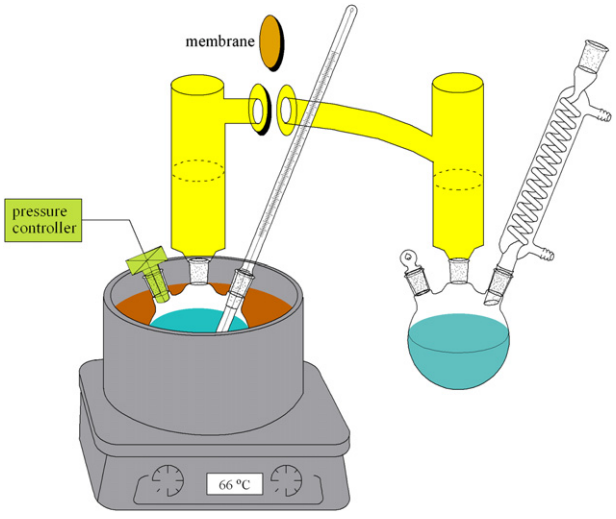

Scheme 2. Apparatus for the measurement of permeability of methanol vapor.

For the dehydrated BPO_4–ABPBI nanocomposite membranes, quite different cross-sectional morphologies are observed compared to that of the dehydrated pristine ABPBI membranes (Fig. 1c and d). The bending and breaking method results rougher cross-sectional surface for the dehydrated BPO_4–ABPBI nanocomposite membranes than that for the dehydrated pristine ABPBI membranes. Bean sprout like structures with characteristic dimension of about 100 nm are observed on the cross-sectional surface (Fig. 1c). For cross-sectional surface of the dehydrated BPO_4–ABPBI nanocomposite membranes prepared using the evaporation and liftoff process, the morphologies are similar however with smaller characteristic dimension than that prepared using the direct liftoff process. Therefore, by controlling the quantity of solvent eliminated from the wet membrane before the liftoff in deionized water, the porosity of the membrane can be controlled. If low porosity is desired, the solvent should be eliminated from the wet membrane before liftoff. The membrane with lower porosity absorbs less phosphoric acid, possesses lower proton conductivity, but higher mechanical strength. On the other hand, the membrane with higher porosity absorbs more phosphoric acid, possesses higher proton conductivity, but lower mechanical strength.

Smooth cross-sectional surfaces were observed for membranes after being doped with phosphoric acid (Fig. 1e–g). The differences in cross-sectional morphologies between that of phosphoric acid doped pristine ABPBI and BPO_4–ABPBI nanocomposite membranes are insignificant as all the nanostructures disappear. In one of SEM morphologies of the phosphoric acid doped BPO_4–ABPBI nanocomposite membranes, a skin-like structure is stripped off from the cross-sectional surface during the treatment of the sample before SEM observation, and sponge-like structure exposes (Fig. 1g). The sponge-like structure not only guarantees the greatest amount of phosphoric acid being soaked in the membrane, but also allows the maximum contact between the membrane matrix and the soaked H_3PO_4. Since no BPO_4 nanoparticles are observed from all the cross-sectional surfaces, it is concluded that the distribution of BPO_4 nanoparticles in the membrane is even; and the BPO_4 nanoparticles are dispersed in the membrane matrix without significant difference from the matrix background.

3.2. FTIR spectroscopy

The FTIR spectra for BPO_4, pristine ABPBI and BPO_4–ABPBI nanocomposite membranes are shown in Fig. 2. The BPO_4 exhibits three strong bands: one band shows two peaks at 565 and 625 cm^{-1} due to the bending vibrations v_4 (F2) of the $[PO_4]^{3-}$ tetrahedron, and the others are at 928 due to the pseudo-lattice translations of B–O and at 1090 cm^{-1} due to the asymmetric stretching vibrations v_3 (F2) of $[PO_4]^{3-}$ tetrahedron, in good agreement with the FTIR of BPO_4 reported in the literature [52]. For the FTIR of pristine ABPBI, the broad band at 3150 cm^{-1} is resulted from the hydrogen-bonded N–H stretching [29,53], and the peaks at 1630, 1580 and 1440 cm^{-1} are attributed to the C=N and C=C stretching [53,54]. The FTIR spectra for BPO_4–ABPBI nanocomposite membranes are similar to that of the pristine ABPBI membrane, indicating that the BPO_4–ABPBI nanocomposite membranes are simply mixture of BPO_4 and ABPBI without significant chemical interaction.

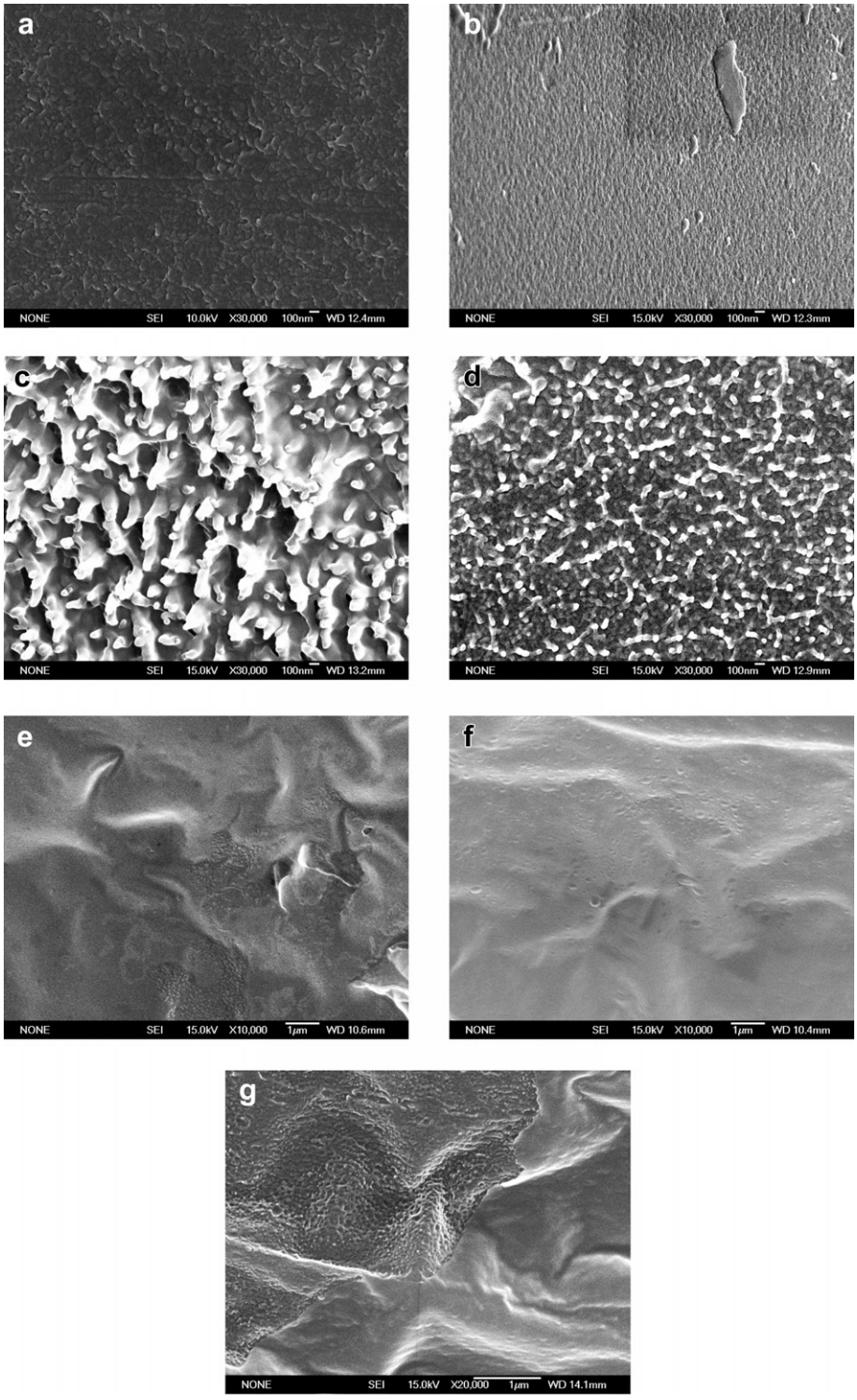

Fig. 1. Cross-sectional morphologies of the dehydrated pristine ABPBI membranes prepared using (a) The direct liftoff process and (b) The evaporation and liftoff process; of the dehydrated BPO_4(25%)–ABPBI nanocomposite membranes prepared using (c) The direct liftoff process and (d) The evaporation and liftoff process; (e) phosphoric acid doped pristine ABPBI membrane prepared using direct liftoff process, (f–g) phosphoric acid doped BPO_4(25%)–ABPBI nanocomposite membranes prepared using the evaporation and liftoff process. All the cross-sectional surfaces were prepared by the bending and breaking method in liquid nitrogen.

3.3. Proton conductivity

The proton conductivities of the membranes were evaluated from the electrical impedance spectroscopy using the two-probe method in temperature range of 100–180 °C by fitting to an equivalent electrical circuit as shown in Fig. 3a. The equivalent electrical circuit is composed of a resistor R_0 representing the membrane resistance, the contact resistors R_1 and R_2, the contact capacitors C_1 and C_2, and the inductor L_0 representing inductance from the platinum leads. The inductance is insignificant as the shielding cable was used. The typical value of resistor R_0 is 1 Ω or less, contact resistor is about 20 kΩ, contact capacitor is about 50 μF,

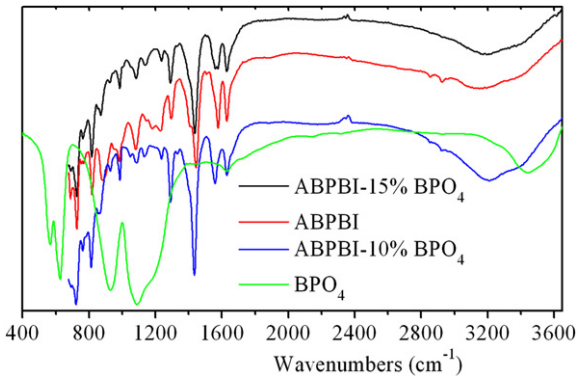

Fig. 2. FTIR spectra of BPO_4, the pristine ABPBI, and BPO_4-ABPBI nanocomposite membranes.

and inductor is about 0.01 μH. At high frequency, the contact capacitors work as short circuits, and the membrane resistance R_0 can be evaluated from the high frequency limit of the circuit resistance.

The typical electrical impedance spectra are shown in Fig. 3b and c. At high frequency, both the real and imaginary parts of electrical impedance are low. As the frequency decreases, both the real and imaginary parts of the impedance increase. At high temperature, the imaginary part of the impedance increases more rapidly than the real part; while at low temperature, the imaginary part of the impedance increases less rapidly than the real part. In our measurement, the membrane resistance R_0 is read from the intercept of the electrical impedance spectroscopy on the real impedance axis Z′ at high frequency.

The temperature dependence of proton conductivity reveals an activated process for both the phosphoric acid doped pristine ABPBI and BPO_4–ABPBI nanocomposite membranes in temperature range of 100–180 °C (Fig. 4). Furthermore, the activation energy is strongly dependent on the thermal treatment history of the membranes (Table 1). For the phosphoric acid doped pristine ABPBI membrane, the proton conductivity varies between 0.13 and 8.51 mS cm^{-1}, with an activation energy of 0.230 eV and pre-exponential factor of 2.74 S cm^{-1}. If the membrane is thermal treated at 180 °C for 3 h under anhydrous environment; the conductivity decreases to about 70% of the untreated one. If 15% of BPO_4 is blended into the ABPBI, the activation energy for proton conducting decreases to about 0.134 eV, and preexponential factor also decreases to 0.094 S cm^{-1} indicating the existence of low concentration of conducting protons with low activation energy. If 25% of BPO_4 is blended to the ABPBI, the activation energy increases to about 0.156 eV and the preexponential factor almost increases for 10 times compared to the membrane containing only 15% BPO_4, indicting the concentration of conducting protons increases. Thermal treatment of the BPO_4–ABPBI nanocomposite membranes under anhydrous environment results the same tendency as that for pristine ABPBI membranes: both the activation energy and the preexponential factor decrease. The maximum conductivity for 25% BPO_4–ABPBI nanocomposite membrane is 27.3 mS cm^{-1} at 180 °C.

3.4. The tensile strength

For the undoped ABPBI and BPO_4–ABPBI nanocomposite membranes, the ultimate tensile strengths are 62.0 and 47.5 MPa; and their Young's moduli are 1064 and 628 MPa. The doping of phosphoric acid enhances the proton conductivity of the ABPBI and BPO_4–ABPBI nanocomposite membranes, while degrades the mechanical properties. The more the phosphoric acid is doped into the membranes, the poorer the mechanical property is. For the phosphoric acid doped ABPBI and BPO_4–ABPBI, their ultimate tensile strengths are 10.1 and 7.5 MPa; and their Young's moduli are 174 and 78 MPa.

In the literature, the tensile strength for undoped ABPBI varies from 88 to 121 MPa depending on degree of polymerization [50]. However, the mechanical properties are very sensitive to the doping level of phosphoric acid. For example, the reported strength at break of the phosphoric acid doped ABPBI is 0.6 MPa and the

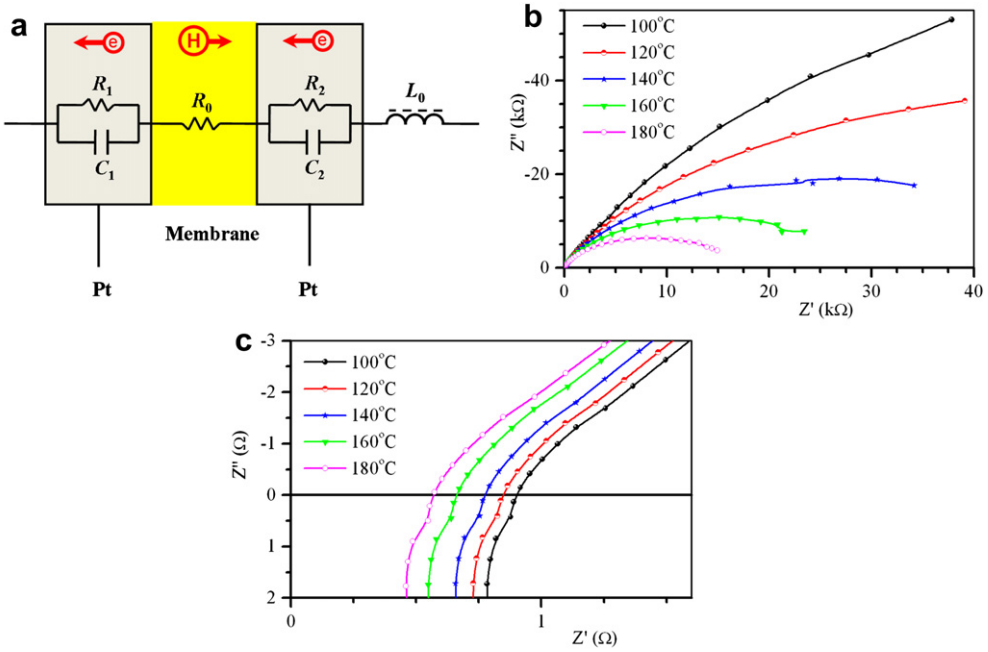

Fig. 3. (a) The equivalent electrical circuit of the two-probe method; (b, c) The typical electrical impedance spectroscopy of phosphoric acid doped ABPBI and BPO_4–ABPBI nanocomposite membranes.

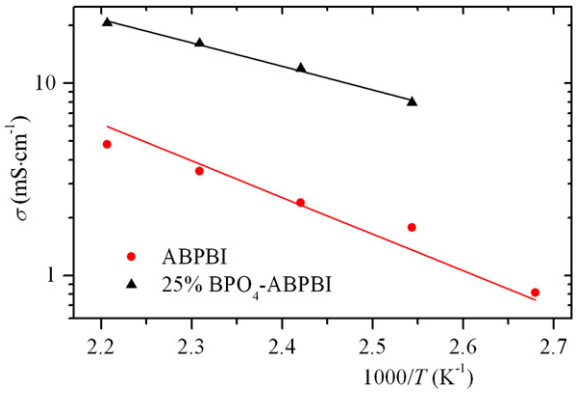

Fig. 4. Temperature dependence of proton conductivity of the phosphoric acid doped pristine ABPBI and BPO_4–ABPBI nanocomposite membranes.

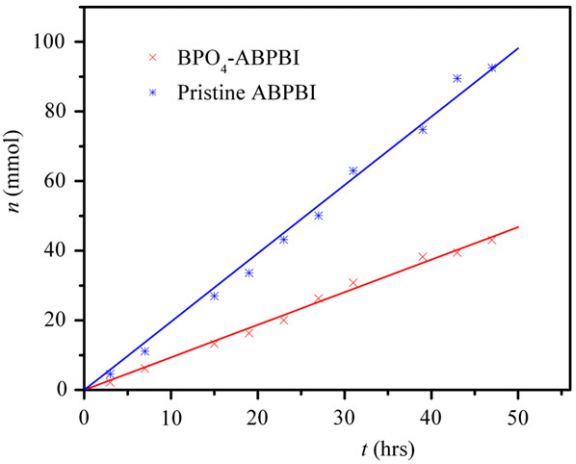

Fig. 5. The moles of methanol vapor that permeates the proton exchange membrane at 65.0 °C; the area and thickness of the membrane are 3.14 cm^2 and 40 μm, respectively.

reported Young's modulus is 2.38 GPa [55]; while in another paper, the Young's moduli of ABPBI prepared by low-temperature casting are 0.290 and 0.104 GPa before or after phosphoric acid doping [56].

3.5. The permeability of methanol vapor

The moles of methanol vapor that permeates the membrane is,

$$n = P\frac{A\Delta p}{d}t \quad (1)$$

where P is the permeability, Δp is the partial pressure difference of the methanol vapor across the membrane, A and d are the area and the thickness of the membrane, and t is the time elapsed during the measurement. The membrane samples for methanol permeability measurements were pretreated the same way as that of other characterization. The moles of methanol vapor that permeates the membrane were shown as a function of elapsed time in Fig. 5; and excellent linear relationships were observed for both the phosphoric acid doped pristine ABPBI and BPO_4–ABPBI nanocomposite membranes. By fitting the experimental data into equation (1), the methanol permeabilities through the phosphoric acid doped ABPBI membranes and the BPO_4–ABPBI nanocomposite membranes were evaluated at 1.71×10^{-14} or 8.17×10^{-15} mol cm cm^{-2} s^{-1} Pa^{-1}, respectively. A two-fold improvement in blocking methanol permeation was observed after the blending of BPO_4 into the phosphoric acid doped ABPBI membranes.

3.6. Discussions

The proton conductivities of phosphoric acid doped ABPBI membranes vary with their preparation procedures, phosphoric acid and moisture contents, and temperatures [29]. The typical conductivity values are about 15 mS cm^{-1} at temperatures as high as 180 °C under anhydrous conditions for MSA/H_3PO_4 direct cast ABPBI/3.0 H_3PO_4 membranes. MSA-cast membranes under the same anhydrous conditions prepared by the soaking method show a conductivity of 25 mS cm^{-1} for ABPBI/2.7 H_3PO_4 at 180 °C, higher than the conductivity obtained for the membranes direct cast from ABPBI/MSA/H_3PO_4 solutions [29]. Kim et al. have reported higher conductivities of 26 mS cm^{-1} for ABPBI/1.6 H_3PO_4, 41 mS cm^{-1} for ABPBI/2.4 H_3PO_4, and 60 mS cm^{-1} for ABPBI/3.7 H_3PO_4 at 110 °C [50]. Although the proton conductivity increases with the increase in phosphoric acid content; the mechanical properties of membrane degrade with the increase in phosphoric acid content. Therefore, it is important to develop novel method to improve the proton conductivity other than to increase the phosphoric acid content.

In this study, the proton conductivity of phosphoric acid doped ABPBI is improved by blending of BPO_4 nanoparticles. For contrast, exactly the same procedures are applied to the preparation of phosphoric acid doped ABPBI or phosphoric acid doped BPO_4–ABPBI nanocomposite with the preblending process. The BPO_4–ABPBI nanocomposite membrane possesses higher conductivity exactly under the same conditions and lower activation energies than the membrane without the blending of BPO_4. The enhancement in proton conductivity by blending of BPO_4 is attributed to the interaction between the BPO_4 and H_3PO_4 since the phosphoric acid attached to the surface of BPO_4 is ready to be ionized thus reducing the activation energy. For example, the conductivity of BPO_4 increases with the increase in B/P ratio as the number of surface P–OH groups increases with the increase in B/P ratio [40]. In Fig. 6, it shows the self-deprotonation Gibbs free energy of phosphoric acid calculated at B3LYP/6-311++G(D, P)/PCM(H_3PO_4) level of theory. The self-deprotonation Gibbs free energy of phosphoric acid in pure phosphoric acid is about 1.12 eV; and this value decreases to about 0.37 eV if a boric acid molecule exists in the vicinity of the phosphoric acid molecule. Therefore it is concluded that the blending of BPO_4 can significantly improve the proton conductivity of phosphoric acid doped ABPBI membranes.

The methanol permeabilities through the phosphoric acid doped ABPBI or BPO_4–ABPBI nanocomposite are significantly larger than that through the phosphoric acid doped PBI on the order of 6.69×10^{-16} mol cm cm^{-2} s^{-1} Pa^{-1} [7]. This difference can be attributed to the rigidity of molecular backbone of ABPBI compared to that of PBI, thus allowing fast diffusion of methanol in the membrane. However, the blending of BPO_4 to ABPBI significantly decreases the methanol vapor permeability through the phosphoric acid doped ABPBI membrane.

Table 1
Proton conducting activation energy e_a and preexponential factor A for the phosphoric acid doped pristine ABPBI and BPO_4–ABPBI nanocomposite membranes.

Membranes	Thermal treatment (°C/hours)	A (S cm^{-1})	E_a (eV)
ABPBI	70/3	2.74	0.230
ABPBI	180/3	1.89	0.233
15% BPO_4–ABPBI	70/3	0.094	0.134
25% BPO_4–ABPBI	70/3	0.924	0.156
25% BPO_4–ABPBI	180/3	0.459	0.134
25% BPO_4–ABPBI	180/24	0.0247	0.111

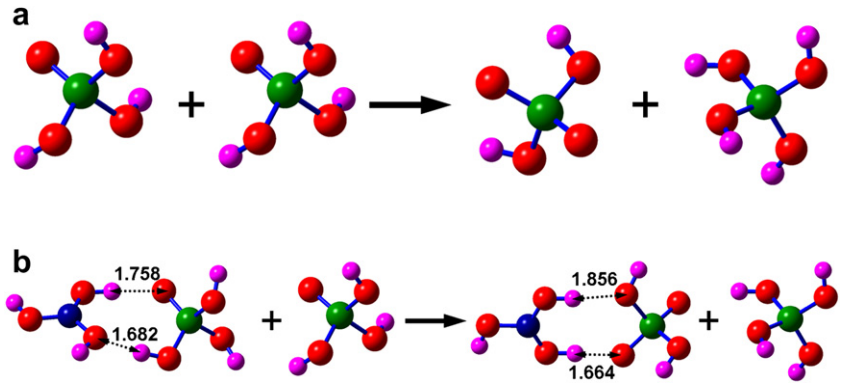

Fig. 6. (a) The self-dissociation Gibbs free energy of 1.12 eV for phosphoric acid is higher than (b) that of 0.37 eV for phosphoric acid in direct contact with a boric acid molecule (color code: red for O, green for P, purple for H, and blue for B). (For interpretation of the references to color in this figure legend, the reader is referred to the web version of this article.)

4. Conclusions

The phosphoric acid doped BPO_4–ABPBI nanocomposite membranes have been successfully prepared by polycondensation of DABA in MSA, either by a preblending or a post-blending process. The BPO_4 nanoparticles are dispersed evenly in the ABPBI matrix forming a nanocomposite membrane with sponge-like morphology after being doped with phosphoric acid. Improved proton conductivity is observed in the phosphoric acid doped BPO_4–ABPBI nanocomposite membrane compared to the phosphoric acid doped pristine ABPBI membrane because of lowered activation energy for proton conducting. The improved proton conductivity is attributed to the dangling hydroxyl or geminal hydroxyl groups of the excess phosphoric acid molecules on surface of BPO_4. The activation Gibbs free energy of these dangling hydroxyl or geminal hydroxyl groups is lower than that of phosphoric acid in the bulk as confirmed by density functional theory calculations. A maximum conductivity of 27.3 mS cm^{-1} at 180 °C is observed for the 25% BPO_4–ABPBI nanocomposite membrane. Finally, the blending of BPO_4 significantly decreases the methanol vapor permeability through the membrane by about two-fold.

Acknowledgments

The authors thank the Laboratory for Microstructures, Shanghai University for carrying out the structural characterization, and acknowledge the financial support from the Chinese National Science Foundation (Nos. 20873081, and 21073118), the Nano project (No. 0952nm01300) of Shanghai Municipal Science & Technology Commission, and the Shanghai Leading Academic Discipline Project (No. J50101).

Appendix A. Supplementary material

Supplementary data related to this article can be found online at doi:10.1016/j.jpowsour.2012.03.091.

References

[1] J. Zhang, Z. Xie, J. Zhang, Y. Tang, C. Song, T. Navessin, Z. Shi, D. Song, H. Wang, D.P. Wilkinson, Z.-S. Liu, S. Holdcroft, J. Power Sources 160 (2006) 872–891.
[2] P.M. Grant, Nature 424 (2003) 129–130.
[3] C. Yang, P. Costamagna, S. Srinivasan, J. Benziger, A.B. Bocarsly, J. Power Sources 103 (2001) 1–9.
[4] V.R. Stamenkovic, B. Fowler, B.S. Mun, G. Wang, P.N. Ross, C.A. Lucas, N.M. Markovic, Science 315 (2007) 493–497.
[5] R. Savinell, E. Yeager, D. Tryk, U. Landau, J. Wainright, D. Weng, K. Lux, M. Litt, C. Rogers, J. Electrochem. Soc. 141 (1994) L46–L48.
[6] Q. Li, R. He, J.-A. Gao, J.O. Jensen, N.J. Bjerrum, J. Electrochem. Soc. 150 (2003) A1599–A1605.
[7] J.S. Wainright, J.-T. Wang, D. Weng, R.F. Savinell, M. Litt, J. Electrochem. Soc. 142 (1995) L121–L123.
[8] L. Yan, X. Ji, W. Lu, J. Phys. Chem. B 112 (2008) 5602–5610.
[9] L. Yan, C. Shao, X. Ji, J. Comp. Chem. 30 (2009) 1361–1370.
[10] C. Shao, L. Yan, X. Ji, S. Zhu, J. Chem. Phys. 131 (2009) 4901–4908.
[11] Y.-T. Kim, K.-H. Kim, M.-K. Song, H.-W. Rhee, Curr. Appl. Phys. 6 (2006) 612–615.
[12] Y. Zhai, H. Zhang, J. Hu, B. Yi, J. Membr. Sci. 280 (2006) 148–155.
[13] V. Tricoli, F. Nannetti, Electrochim. Acta 48 (2003) 2625–2633.
[14] S.R. Samms, S. Wasmus, R.F. Savinell, J. Electrochem. Soc. 143 (1996) 1225–1232.
[15] R. Bouchet, E. Siebert, Solid State Ionics 118 (1999) 287–299.
[16] X. Glipa, B. Bonnet, B. Mula, D.J. Jones, J. Rozière, J. Mater. Chem. 9 (1999) 3045–3049.
[17] M. Kawahara, J. Morita, M. Rikukawa, K. Sanui, N. Ogata, Electrochim. Acta 45 (2000) 1395–1398.
[18] D. Zhang, L. Yan, J. Phys. Chem. B 114 (2010) 12234–12241.
[19] L. Yan, S. Zhu, X. Ji, W. Lu, J. Phys. Chem. B 111 (2007) 6357–6363.
[20] R. He, Q. Li, G. Xiao, N.J. Bjerrum, J. Membr. Sci. 226 (2003) 169–184.
[21] O. Nakamura, T. Kodama, I. Ogino, Y. Miyake, Chem. Lett. 8 (1979) 17–18.
[22] P. Staiti, J. New Mat. Electrochem. Syst. 4 (2001) 181–186.
[23] S. Feng, Y. Shang, S. Wang, X. Xie, Y. Wang, Y. Wang, J. Xu, J. Membr. Sci. 346 (2010) 105–112.
[24] J.K. Lee, J. Kerres, J. Membr. Sci. 294 (2007) 75–83.
[25] H. Pu, L. Liu, Z. Chang, J. Yuan, Electrochim. Acta 54 (2009) 7536–7541.
[26] Y. Oono, A. Sounai, M. Hori, J. Power Sources 189 (2009) 943–949.
[27] A. Verma, K. Scott, J. Solid State Electrochem. 14 (2010) 213–219.
[28] H.-S. Lee, A. Roy, O. Lane, J.E. McGrath, Polym 49 (2008) 5387–5396.
[29] J.A. Asensio, P. Gómez-Romero, Fuel Cells 5 (2005) 336–343.
[30] C. Wannek, W. Lehnert, J. Mergel, J. Power Sources 192 (2009) 258–266.
[31] P. Krishnan, J.S. Park, C.S. Kim, J. Power Sources 159 (2006) 817–823.
[32] S. Zhu, L. Yan, D. Zhang, Q. Feng, Polymer 52 (2011) 881–892.
[33] J.A. Asensio, S. Borrós, P. Gómez-Romero, Electrochim. Acta 49 (2004) 4461–4466.
[34] S.K. Kim, T.H. Kim, J.W. Jung, J.C. Lee, Macromol. Mater. Eng. 293 (2008) 914–921.
[35] P. Gómez-Romero, J.A. Asensio, S. Borrós, Electrochim. Acta 50 (2005) 4715–4720.
[36] J.A. Asensio, S. Borrós, P. Gómez-Romero, Electrochem. Commun. 5 (2003) 967–972.
[37] O. Acar, U. Sen, A. Bozkurt, A. Ata, Int. J. Hydrogen Energy 34 (2009) 2724–2730.
[38] S. Yu, H. Zhang, L. Xiao, E.W. Choe, B.C. Benicewicz, Fuel Cells 9 (2009) 318–324.
[39] A. Sannigrahi, D. Arunbabu, R.M. Sankar, T. Jana, J. Phys. Chem. B 111 (2007) 12124–12132.
[40] S.D. Mikhailenko, J. Zaidi, S. Kaliaguine, J. Chem. Soc. Faraday Trans. 94 (1998) 1613–1618.
[41] S.D. Mikhailenko, S.M.J. Zaidi, S. Kaliaguine, Catal. Today 67 (2001) 225–236.
[42] I.S. Mulla, V.A. Chaudhary, K. Vijayamohanan, Sensors Actuators A: Phys. 69 (1998) 72–76.
[43] M.H.D. Othman, A.F. Ismail, A. Mustafa, J. Membr. Sci. 299 (2007) 156–165.
[44] E. Cho, J.-S. Park, S.-H. Park, Y.-W. Choi, T.-H. Yang, Y.-G. Yoon, C.-S. Kim, W.-Y. Lee, S.-B. Park, J. Membr. Sci. 318 (2008) 355–362.
[45] P. Krishnan, J.-S. Park, C.-S. Kim, J. Membr. Sci. 279 (2006) 220–229.
[46] S. Wen, C. Gong, W.-C. Tsen, Y.-C. Shu, F.-C. Tsai, Int. J. Hydrogen Energy 34 (2009) 8982–8991.
[47] Y.F. Liang, X.L. Zhu, X.G. Jian, Solid State Ionics 179 (2008) 1940–1945.
[48] S.-H. Park, J.-S. Park, S.-D. Yim, S.-H. Park, Y.-M. Lee, C.-S. Kim, J. Power Sources 181 (2008) 259–266.
[49] S.M.J. Zaidi, Electrochim. Acta 50 (2005) 4771–4777.

[50] H.-J. Kim, S.Y. Cho, S.J. An, Y.C. Eun, J.-Y. Kim, H.-K. Yoon, H.-J. Kweon, K.H. Yew, Macromol. Rapid Comm. 25 (2004) 894–897.
[51] X.-L. Zhou, Yunnan Chem. Technol. 37 (2010) 15–18.
[52] S. Chen, M. Ye, H.-H. Chen, X.-X. Yang, J.-T. Zhao, J. Inorg. Organomet. Polym. Mater. 19 (2009) 139–142.
[53] J.A. Asensio, S. Borros, P. Gomez-Romero, J. Electrochem. Soc. 151 (2004) A304–A310.
[54] O. Acar, U. Sen, A. Bozkurt, A. Ata, J. Mater. Sci. 45 (2010) 993–998.
[55] H. Zheng, L. Petrik, M. Mathe, Int. J. Hydrogen Ener. 35 (2010) 3745–3750.
[56] E.A. Franceschini, H.R. Corti, J. Power Sources 188 (2009) 379–386.